PCCP

The set of valley–ridge inflection points on the potential energy surface of water

Michael Hirsch,[a] Wolfgang Quapp*[a] and Dietmar Heidrich[b]

[a] *Mathematisches Institut, Universität Leipzig, Augustus-Platz, D-04109 Leipzig, Germany. E-mail: quapp@server1.rz.uni-leipzig.de*
[b] *Wilhelm Ostwald Institut für Physikalische und Theoretische Chemie, Universität Leipzig, D-04109 Leipzig, Germany*

Received 22nd July, Accepted 4th October 1999

The MP2/6-31G** potential energy surface (PES) of the water molecule is used as a model to locate curves of valley ridge inflection (VRI) points. Crossing points between VRI curves and approximations of the reaction path allow the identification of a symmetric bifurcation of the reaction path. The VRI points are calculated with the help of Branin's method. The recently proposed method of following the reduced gradient is used to calculate reaction path approximations of "inversion" and dissociation together with their possible bifurcations. The results gained by a model PES (W. Quapp, M. Hirsch and D. Heidrich, *Theor. Chem. Acc.*, 1998, **100**, 285) are now confirmed by the *ab initio* surface of the water molecule. We discuss the chemical and physical meaning of VRI curves in terms of the fourfold cluster problem of highly excited rotational states; the core area of our surface is of sufficient quality for this.

1 Introduction

Branching reaction paths is a frequently discussed event in chemistry but the calculation of branching points still remains a challenge for theoretical chemistry. We seek to understand branching in terms of the potential energy surface (PES) which also forms the basis for the conventional transition state theory.[1] Branching of a reaction path leads to the formation of alternative reaction channels on the PES describing the chemical reaction. Some aspects of the bifurcation have allready been discussed in earlier publications.[2–4] The methods of PES analysis[5–7] form the tool to identify the branching of the reaction path. Furthermore, the choice of the path definition is important. The reaction path is an assumed curve in the configuration space of the PES connecting the reactant with one or more products with the help of the corresponding saddle point (SP) along the so-called minimum energy path (MEP). This way, the MEP is the leading line characterizing the reaction channel in which the trajectories, or, in terms of quantum mechanics, the wave packets should move. However, the term MEP is not yet sufficiently specified to determine a curve uniquely for the reaction path. There are several possibilities to define a reaction path mathematically. The most important definitions are either the steepest descent from the saddle or the gradient extremal which follows the least ascent. Pathways corresponding to different definitions usually branch at different points of the configuration space. On the other hand, the PES shows points which we intuitively connect with the branching of the reaction path but which do not depend on any reaction path definition. They are defined by the characteristics of the PES itself. Such points are the valley–ridge inflection (VRI) points[8] and we will differentiate between these two kinds of points.

The steepest descent from the SP in mass-weighted Cartesian coordinates is the simplest definition of a reaction path, which is well-known as the intrinsic reaction coordinate (IRC).[9–10] The pathway is given by an autonomous system of differential equations using the negative gradient of the PES for the tangent vector of the curve. The gradient is the zero vector at stationary points. With the exception of the stationary points the solution of the differential equation of the IRC is unique. So, the IRC cannot bifurcate[11] and consequently the IRC method is not well-adapted to tackle the problem of branching reaction paths.

Gradient extremals[12–14] form a second possibility for defining a reaction path. The calculation of the gradient extremal is much more complicated in comparison with the IRC, but the gradient extremal is defined locally. Furthermore, the gradient extremal can bifurcate.[15,16] However, gradient extremals often leave the valley ground and avoid an assumed branching by passing a turning point. Frequently, a pair of turning points at both sides of the assumed branching point exist. This problem will not be discussed here.

A third possibility for defining a pathway between minimum and saddle point is the method of "following the reduced gradient" (RGF).[17] Here a curve is generated with a constant gradient direction at every point along the pathway. Such directions can always be selected to coincide with the development of any reaction, *i.e.* with the main directions of the harmonic potential, the normal modes. There has always been a field of such curves from which the most suitable curve may be selected. It seems interesting that the RGF method includes the distinguished coordinate method.[6,18] Thus, a certain number of curves calculated by RGF for well-selected directions may offer good approximations for reaction paths. To be more precise, the beginning of such a curve has to be stated as a MEP which follows one of the main directions of the harmonic potential at a minimum. After the starting phase the curve continues and may reach a SP, although it does not exactly fulfill the criteria of a MEP. This third possibility to follow a reaction path is treated in this paper, because the branching points of the reduced gradient curve are actually the VRI points of the PES. The VRI points gain importance when tackling the problem of reaction path branching.

As already reported,[19] the VRI points may form a manifold in the configuration space of the chemical species. This manifold can have the dimension $N-2$, if the configuration space of the PES has dimension N.[20] Hence, to find such manifolds, test surfaces with a dimension higher than $N=2$ are needed. In ref. 19 we have discussed a 3-dimensional test surface and

now we will turn to the quantum chemically determined PESs of real molecules. The MP2/6-31G** *ab initio* PES of the water molecule is used to show the existence, the characteristics and the possible meaning of VRI points for locating branching points along possible reaction channels ("dissociation"). A 1-dimensional manifold of VRI points is found. It is obvious that the quantum chemical level used is not sufficient to give a globally correct surface of the H_2O molecule. Especially, dissociations like $H_2O \rightarrow O + H_2$ cannot be described adequately without using CASSCF or related methods. It is not the objective of this paper to give an exact description of the high-energy parts of the water PES. But, in the region of interest up to an O–H distance of 1.6 Å, the MP2 surface of H_2O is still quite similar to the MR-CI surface of Ho *et al.*[21] In addition, we use the surface as a model for H_2X molecules in order to discuss chemical and spectroscopic problems in a more general sense.

This paper is subdivided as follows: first we will outline the RGF and the global Newton method (Branin method) and show their relationship. Then characteristics of VRI points generated in this way will be examined and the manifold of VRI points of the H_2O PES will be specified. The possible meaning of those curves and of certain points on it are discussed. The appendix outlines a short description of the realisation of the RGF algorithm in internal coordinates.

2 Reduced gradient curves and their branching points

The idea to follow a reduced gradient was introduced in ref. 17. The method is generalised by allowing a free selection of the gradient direction which the curve has to follow (see ref. 19). In this case, the "reduction" is realised by a projection of the gradient onto the $(N-1)$-dimensional subspace which is orthogonal to the 1-dimensional subspace spanned by the search direction $\boldsymbol{r}$, instead of omitting one of the coordinate directions. A curve belongs to the search direction $\boldsymbol{r}$, if the gradient always remains parallel to the direction of $\boldsymbol{r}$ at every point along the curve. Based on an explicit definition, we can follow this curve along its tangential vector. It is proved that the tangent vector is nonzero outside stationary points and VRI points.[22] In contrast to the conventional distinguished coordinate method (cf. ref. 18), a reduced gradient curve passes possible turning points without jumps.

There are two different methods to get a reduced gradient curve: the RGF and the Branin method. These methods are based on several ideas and have different applications in the examination of the PES. The method of RGF is described in ref. 17 and generalised in ref. 19. It is given by the equation

$$\boldsymbol{P}_r \boldsymbol{H} \dot{\boldsymbol{x}} = 0 \qquad (1)$$

where $\boldsymbol{P}_r$ orthogonally projects to the search direction $\boldsymbol{r}$. That means $\boldsymbol{P}_r \boldsymbol{r} = \boldsymbol{0}$. The matrix $\boldsymbol{H}$ is the Hessian, and $\dot{\boldsymbol{x}}$ is the tangent to the curve. In general, the search direction and the tangent are different. The projector $\boldsymbol{P}_r$ does not depend on the coordinates $\boldsymbol{x}$ or on the curve parameter. The algorithm is realized by the predictor-corrector method.[19,23] It is appropriate to detect unknown stationary points, for instance saddle points of index one (transition structures). The method starts at a stationary point, *e.g.* a minimum, and follows an arbitrarily selected direction of the gradient on the PES.

The effort required for RGF lies between that of gradient extremal and IRC following. Each step requires a Hessian matrix or its update. The search for stationary points is the main application of the RGF method. Success does not depend too much on an exact selection of the starting direction and an intuitive selection is usually sufficient.

Because the gradient directions of the PES are uniquely determined, curves calculated by RGF to different directions cross if and only if the gradient vanishes at the crosspoint, *i.e.* the crosspoint has to be a stationary point. However, different branches of the solution of the *same* reduced gradient curve may also cross each other. These points are then characterised as the branching points of the reduced gradient curve, being the VRI points of the surface. Whenever a reduced gradient curve reaches a VRI point, the curve branches and at every VRI point of the PES the solution of a reduced gradient curve branches.[19] The characteristic attribute of a VRI point is the zero eigenvalue of the Hessian. At least one eigenvalue changes its sign when going along the gradient,[8] where the corresponding eigenvector is orthogonal to the gradient. This means that a valley changes into a ridge or *vice versa.*

Properties of curves calculated by RGF are illustrated in Fig. 1. The RGF method is applied to the Müller–Brown potential[24] by using the Mathematica program.[25] Figure 1(a) shows curves belonging to the directions (0.7, −0.3) and (0.7, 0.3) (dashed). Both curves connect all stationary points of the surface, as is the usual property of RGF. The parts of the reduced gradient curve are not necessarily connected. The dashed curve in Fig. 1(b) belonging to the direction (0.65, 0.35) consists of three isolated parts. Nevertheless, all stationary points are reached. This also means that, following an unfavourable starting direction, the curve may not reach the desired stationary point, because it is divided into disconnected parts. However, each closed part of a reduced gradient curve crosses an even number of stationary points.[22] Thus, if the search starts at a stationary point and follows a closed part, it reaches at least another stationary point. The occurrence of a turning point is often an indication of the existence of a VRI point nearby. In such cases there is an adjacent reduced gradient curve to another search direction, which branches at this VRI point [note: not all VRI points of the Müller–Brown surface are marked in Figs. 1(a) and 1(b)]. The

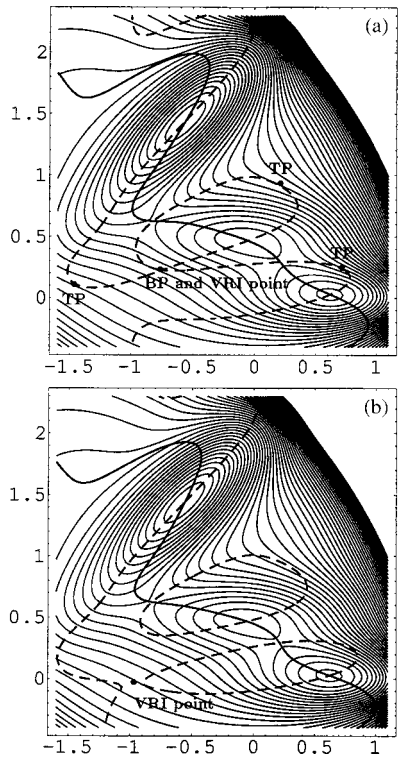

Fig. 1 Müller–Brown Surface[24] with curves obtained by RGF. (a) directions (0.7, −0.3) and (0.7, 0.3) (dashed). All stationary points are connected. The dashed curve branches at a valley–ridge inflection point, VRI. (b) directions (0.65, −0.35) and (0.65, 0.35) (dashed). The dashed curve follows an unfavourable search direction. It reaches each stationary point, but it splits into three isolated parts. The VRI point is indicated by turning points, TP, of the curve. BP means branching point.

solid lines in Figs. 1(a) and 1(b) are well chosen curves for finding all stationary points. They demonstrate that a reduced gradient curve can be chosen to form a good approximation of a reaction path over wide regions of the PES. If a reduced gradient curve directly connects two stationary points without crossing a VRI point, then the indices of the stationary points differ by one.[22] Hence, a VRI point must exist along the reduced gradient curve which connects two SPs of first order. (These statements are made under the assumption that the stationary points are not the VRI point.)

The RGF method is related to the well-known mathematical theory of Branin,[26] the so-called global Newton method.[20] Its application to PES analysis has been described in ref. 19. The procedure uses the adjoint $\boldsymbol{A}$ of the Hessian $\boldsymbol{H}$. It is defined by the equation $\boldsymbol{AH} = \mathrm{Det}(\boldsymbol{H})\boldsymbol{I}$, where $\boldsymbol{I}$ is the unit matrix. The global Newton method defines an autonomous system of differential equations for the curve $\boldsymbol{x}(t)$, where t is a curve length parameter:

$$\dot{\boldsymbol{x}} = \mp\mu\boldsymbol{A}(\boldsymbol{x})\boldsymbol{g}(\boldsymbol{x}), \qquad (2)$$

applied as $$\boldsymbol{x}_{m+1} = \boldsymbol{x}_m \mp \Delta t\boldsymbol{A}(\boldsymbol{x}_m)\boldsymbol{g}(\boldsymbol{x}_m)$$

The sign in eqn. (2) determines the index of the stationary point which we are searching for. The negative sign stands for stationary points of even index, *i.e.* minima or second order SPs. The positive sign stands for stationary points of odd index, among them first order SPs (transition structures). The Branin method does not need any corrector step and the calculation can be stopped and restarted at any time. Thus, it is possible to change the steplength parameter, Δt, and to continue the calculation at the last point. The steplength of the Branin method depends on the adjoint of the Hessian and the gradient. If the product of adjoint and gradient becomes a zero-vector, the steplength is zero. This happens either in stationary points, where the gradient vanishes, or in VRI points. In the second case the determinant of the adjoint of the Hessian vanishes. Hence, stationary points and VRI points are the limits of the Branin method. In mathematical terms, the VRI points are singular points of the Branin method.[20]

The starting point for the Branin method may be any point of the PES, except for stationary points and VRI points, whereas the search direction is given by the gradient at this point. If the search direction of a Branin curve does not exactly coincide with the direction of the gradient at the VRI point (which we search for), a turning point occurs [*cf.* Fig. 1(b)]. Hence, we have to start at a point where the gradient has the same direction as the gradient at the VRI point. This can be realised for manifolds of VRI points in symmetric subspaces of the configuration space. Therefore, a systematic search for VRI points in symmetry planes of the PES of water is possible. In this case, along the pathway of a Branin curve, the eigenvalue of an eigenvector, being orthogonal to the gradient, converges to zero.

Another method to describe a reduced gradient curve is the standard homotopy method as shown in ref. 27, using an additional curve parameter which increases the dimension of the problem by one.

3 The potential energy surface of water

Visualisation by cross sections

The calculations on the H_2O molecule use the MP2/6-31G** method of the Gamess-UK program package.[28] Internal mass-weighted coordinates were used (see Appendix), where r denotes the distance O–H and α the angle H–O–H. As the complete 3-dimensional potential energy hypersurface of H_2O cannot be visualised, we use three types of sections (see Fig. 2). First, the symmetric plane (α, $r_1 = r_2$), second, the antisymmetric planes (α, $r_2 = 2R - r_1$), where R is a fixed O–H distance at $r_1 = r_2$, and third, the (r_1, r_2) planes for a fixed α. All these special planes are perpendicular to each other. The sectional submanifolds of the PES are 2-dimensional surfaces calculated by single-point MP2 calculations over grids of 41 × 41 up to 41 × 81 points in the configuration space. Interpolations are done by Mathematica.[25] The representation of the H_2O PES in the figures is curvilinear, and is thus distorted. The length of the 1 Å arc, with a radius of 1 Å, corresponds nearly to 57°, in non-mass-weighted coordinates. We use a standardised notation, *i.e.* the same letters or numbers in the figures are related to the same object. Furthermore, capitals are used to denote points and regions of the PES, Arabic numerals denote curves.

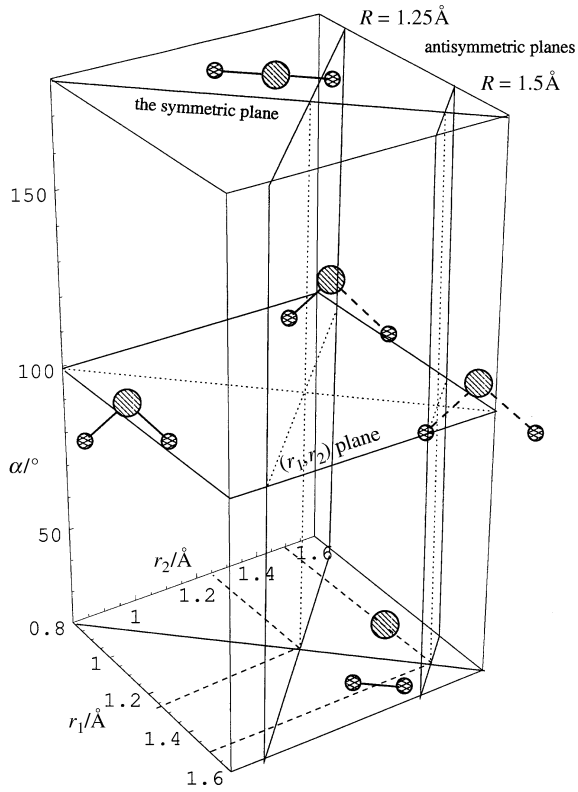

Fig. 2 Configuration space of H_2O with the planes of section, and a display of selected geometries of the water molecule.

Another visualisation: "The Apple"

Illustrating the potential energy of H_2O in a particular manner, a 3-dimensional picture is shown in Fig. 3. The coordinate system used is that of Fig. 2. The centre of the surface is the configuration with the minimum energy. We leave the minimum configuration in steps of equal length (0.05 Å) in every direction. The value of the new potential energy states the distance of the surface point from the centre. Thus, the energy difference between the equilibrium structure and a point at a fixed distance from the equilibrium structure is shown. This definition is analogous to the rotational energy surface, see ref. 29.

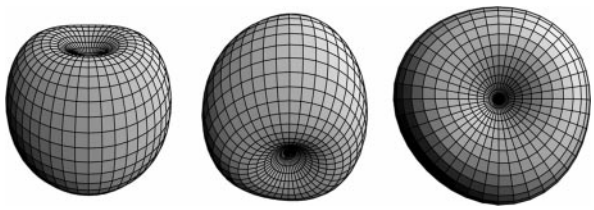

Fig. 3 "The Apple": energy changes by leaving the global minimum of water by equal steps in all directions. The coordinates are the same as in Fig. 2.

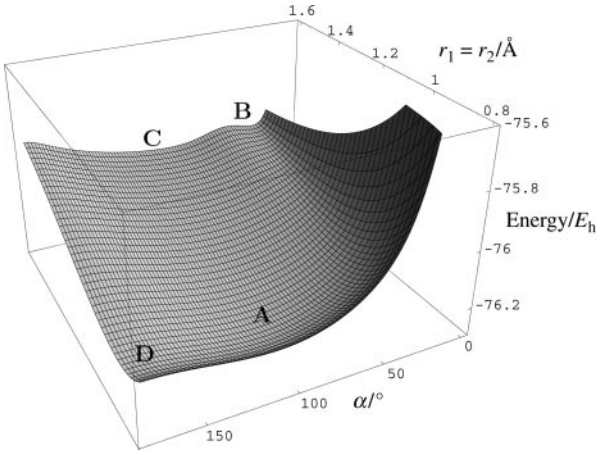

Fig. 4 The symmetric section of the PES of H_2O. Point A: global minimum; region B: the dissociation channel forming $O + H_2$; region C: $O + H + H$ dissociation path; point D: saddle point at the linear structure.

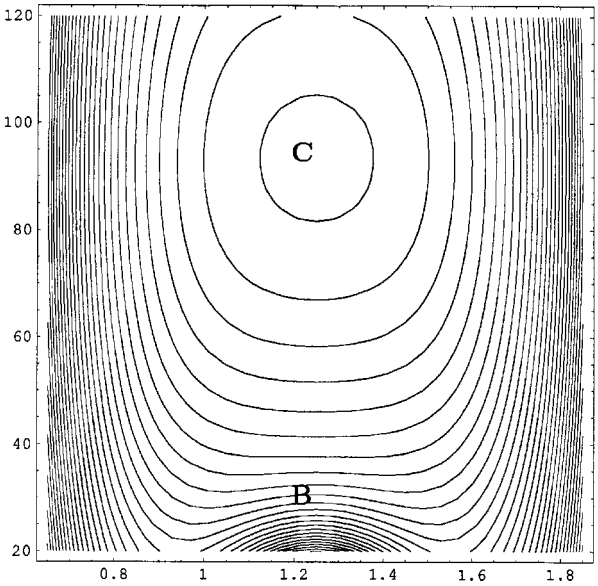

Fig. 5 Antisymmetric section of the PES of H_2O taken at $R = 1.25$ Å.

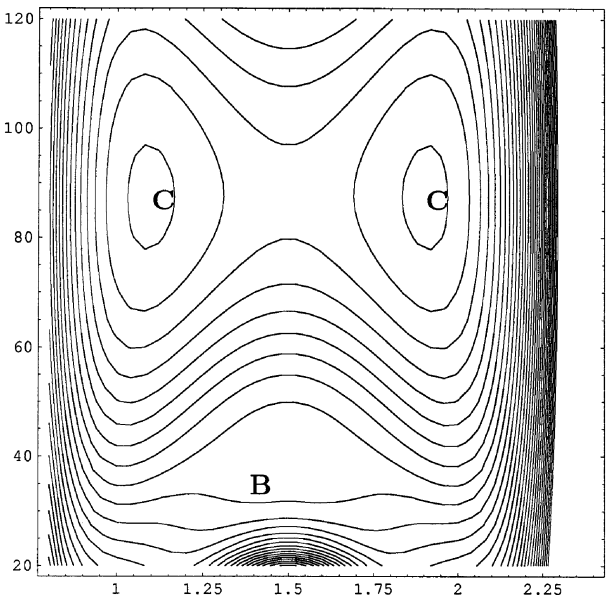

Fig. 6 Antisymmetric section of the PES of H_2O taken at $R = 1.5$ Å (*cf.* Fig. 5). The "eyes" C represent the sections of two branches of the valley leading to H···OH or HO···H, respectively. The "mouth" B is a cross section of the dissociation channel which forms $O + H_2$.

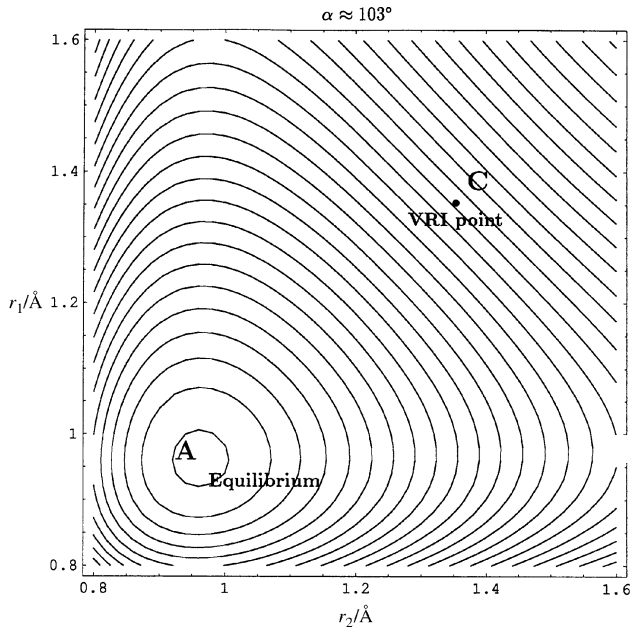

Fig. 7 (r_1, r_2) Section of the PES of H_2O. Point A is the global minimum. The VRI point is near C (where $r_1 = r_2 \approx 1.35$ Å).

The picture depicted in Fig. 3 looks like an apple. The "apple-blossom" and the "apple-stalk" represent the bending mode, which gives the direction of the lowest change of energy. The relation between both the symmetric and the antisymmetric modes can be seen in the on-top view. The symmetric mode lies in the direction from southwest to northeast and the antisymmetric mode from southeast to northwest. It is clearly seen that the "least ascent" MEP starts along the bend direction, whereas the symmetric stretch pathway comes next, being much steeper. The antisymmetric stretch is the strongest vibration, at least near the minimum configuration. The surface may be the 3-dimensional vibrational energy picture of H_2O, seen in an inverse representation in comparison to the usual equipotential surfaces, *cf.* ref. 19.

Topography and reaction channels

Fig. 4 shows the symmetric section of the PES of H_2O. The global minimum is shown by point A (MP2/6-31G**: 0.961 Å, 103.87°, −76.222 449 E_h) and the SP of inversion at $\alpha = 180°$ by point D. Region B is a reaction valley related to the dissociation channel forming $O + H_2$ (note that a MP2 level calculation is not able to represent the whole dissociation process sufficiently). Fig. 4 gives an impression of the MEP starting at the minimum structure shown by A and following the symmetric dissociation channel. Moving from point A to region C, there is another valley-like structure (a "cirque") reaching higher energies. In the MP2 model it represents the $O + H + H$ dissociation. (The classification of valleys or ridges is not important for the discussion of VRI points, *cf.* refs. 30 and 31 and further discussions there.) An antisymmetric section of the PES (Fig. 5), intersecting the symmetry plane at $r_1 = r_2 = 1.25$ Å, shows a symmetric minimum representing the flat valley C of Fig. 4. The dissociation channel B is visible at the bottom of Fig. 5. However, the situation in the antisymmetric section at $R = 1.5$ Å is quite different (Fig. 6). Whereas the "mouth" of the "face" is the analogous section through the dissociation channel B ($O + H_2$), the "eyes" now represent the section of two branches of the flat valley **C**. Hence, the valley C bifurcates between the distances 1.25 and 1.5 Å of the symmetric section. The branching point is a VRI point. It can also be found in the (r_1, r_2) plane shown in Fig. 7 ($\alpha = 103°$). The VRI point is located

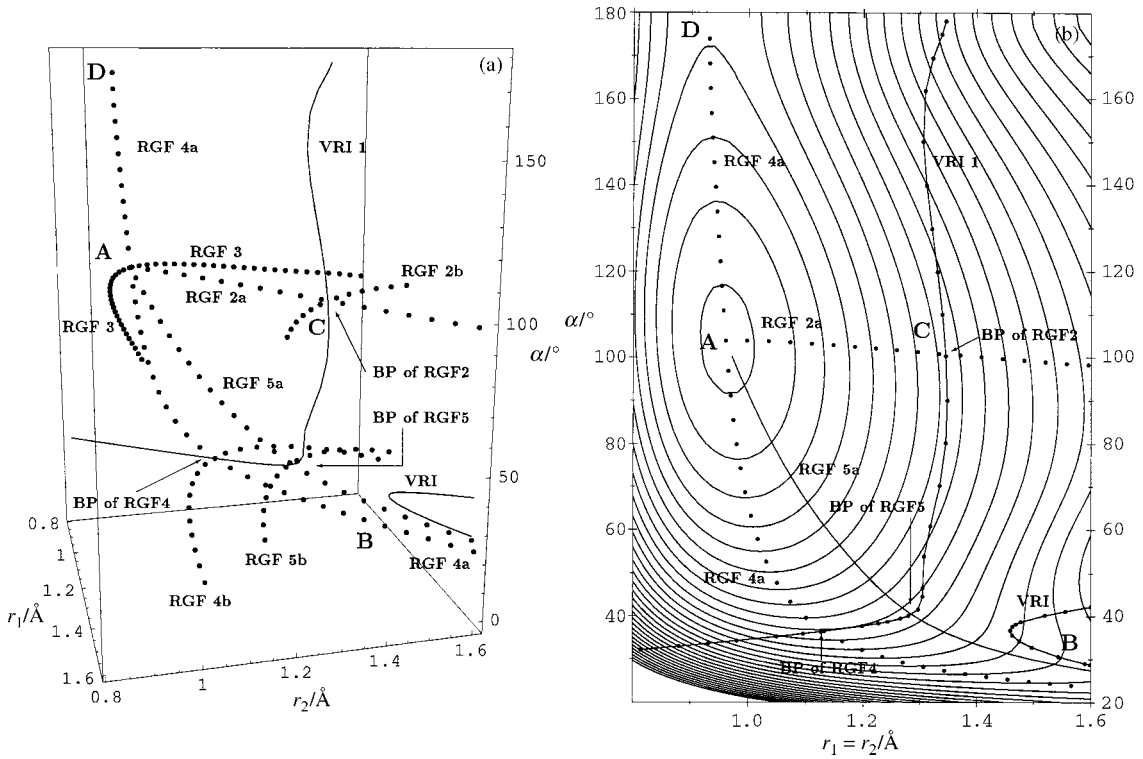

Fig. 8 (a) The configuration space of H_2O. 1: first curve of VRI points; 2a: reduced gradient curve which belongs to the direction of the symmetric stretch; 2b: bifurcation of 2a towards OH + H dissociation; 3: reduced gradient curve to the direction of the antisymmetric stretch; 4a, 4b: the two parts of the reduced gradient curve which belong to the direction of the bend; 5a, 5b: reduced gradient curve approximating the MEP. (b) The symmetric subspace with equipotential lines. Notation is the same as in part a.

near $r_1 = r_2 \approx 1.35$ Å. However, this point is difficult to visualise because of the flatness of the surface in this region.

The two further valleys of Fig. 7, lying parallel to the axes, belong to the antisymmetric stretch mode. It is well known from experiments that this mode changes from a normal mode behaviour (lying diagonal in the potential well) to a local mode along one of the valleys, after sufficient excitation.[32]

4 The set of valley–ridge inflection points on the PES of water

In a previous paper,[19] we used a test surface to show that VRI points may form a manifold of the dimension $\leqslant(N-2)$, where N is the dimension of the configuration space. In other words, for PESs with dimension higher than two, the set of VRI points may be a curve or even a higher-dimensional manifold. Using the Branin method, it is possible to search systematically for VRI points of the PES of symmetric configurations of H_2O. The resulting curves of VRI points of the PES of H_2O are shown in Figs. 8(a) and 8(b) together with other characteristic features of the configuration space and the symmetric subspace. Point A again depicts the global minimum, point D is the SP forming the linear structure and region B is the location of the dissociation channel forming $O + H_2$. Curve 1 is a manifold of VRI points which is shown separately in Fig. 9 together with its energy profile. The VRI point predicted by the two antisymmetric sections (Figs. 5 and 6) is also located on curve 1 in Fig. 8. It is situated at the crossing of the curves 1 and 2 in region C.

The method of calculation can be described as follows: the VRI points forming curve 1 have been calculated by the Branin method using eqn. (2). To find a point, we first fixed a starting point. After convergence to a VRI point, the next initial point is selected, for example along the middle part of curve 1 by changing the angle coordinate by 5°. The sign used in the Branin search depends on the side of the VRI curve where the initial point is located (relative to the global minimum A). If necessary, we can restart the procedure with the opposite sign. The calculated points are listed in Table 1. We use a symmetry restriction for the two r(O–H) distances. If no symmetry is enforced, any small numerical uncertainty in the two O–H distances causes a turn off of the Branin search in the full 3-dimensional configuration space, and the search misses the symmetric VRI point. Such behaviour has already been reported in ref. 19.

In our first presentation[17] the RGF was calculated by following the direction of the internal coordinate axes. A generalisation of the concept was given by the use of any gradient direction in the configuration space.[19] It becomes particularly important for the simulation of normal modes or combination modes at the initial stationary point.[6,7] The procedure corresponds to the well-known method of a distinguished coordinate.[18] The curves 2–4 in Fig. 8 are calculated by the RGF method; they belong to the directions of normal modes at the minimum A: symmetric stretch (curve 2), antisymmetric stretch (curve 3), and the bend mode (curve 4). Notably, normal modes are not necessarily the best choice of the search

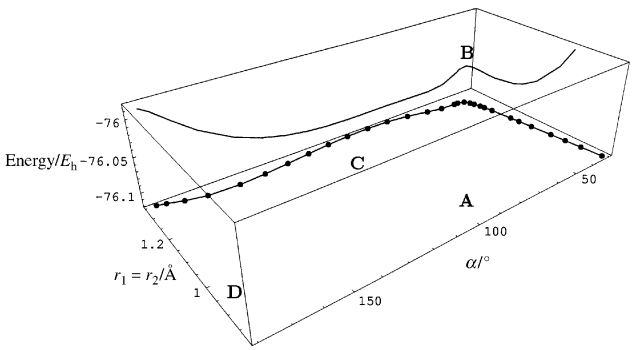

Fig. 9 Energy profile along curve 1 (VRI points) in the symmetric section of the configuration space of H_2O. Capitals are used as in Figs. 4 to 8.

Table 1 VRI points (curve 1) at $r = r_1 = r_2$.

r/Å	α/°	Energy/E_h
0.8142079	32.0898822	−75.79598381
0.8805428	32.9069335	−75.91140887
0.9321274	33.5856487	−75.97170769
0.9809287	34.2509481	−76.01118472
1.0495921	35.2165455	−76.04517464
1.0954554	35.8889383	−76.05734627
1.1261898	36.3619864	−76.06187406
1.1979250	37.6168824	−76.06381851
1.2272689	38.2585028	−76.06197996
1.2432003	38.6730896	−76.06053391
1.2660677	39.4282580	−76.05813829
1.2799648	40.0788024	−76.05673027
1.2969708[a]	41.5297075	−76.05603934
1.3049490	44.5677445	−76.06059859
1.3048634	46.5586749	−76.06481013
1.3075098	53.8655630	−76.07790826
1.3185499	60.8132821	−76.08490366
1.3352569	70.2243254	−76.08942604
1.3457460	80.1428205	−76.09199630
1.3485165	90.0180881	−76.09317728
1.3458742	100.3116099	−76.09245610
1.3398904	109.9777560	−76.08961314
1.3313655	119.8485404	−76.08431447
1.3214642	129.7984578	−76.07627010
1.3118746	139.8510865	−76.06502995
1.3055246	150.0896531	−76.04981237
1.3093429	161.9287987	−76.02622996
1.3231472	169.4424709	−76.00720584
1.3390953	174.9747750	−75.99261526
1.3462948	178.0451248	−75.98698623

[a] Bifurcation part of MEP, see discussion.

direction to approximate a reaction path by a reduced gradient curve whereas curve 5, belonging to a combination mode in Fig. 8, matches the reaction path much better than curve 4 which belongs to the bend mode.

Curve 2 is of great interest. It is composed of two parts. The symmetric part 2a starts at the global minimum, point A, and

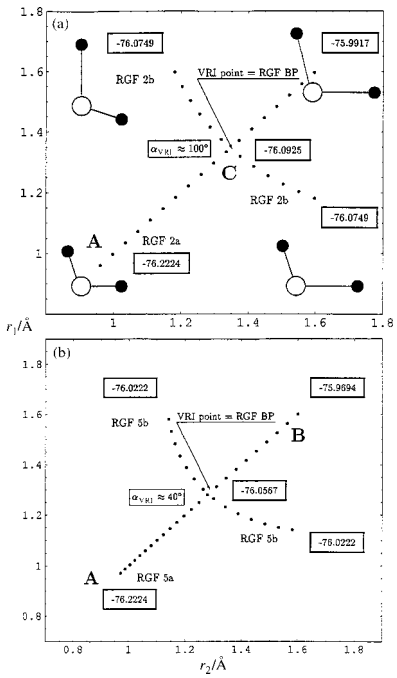

Fig. 10 (a) Projection of reduced gradient curve 2. At the VRI point, the breakdown of symmetry is energetically favourable in comparison with the symmetric pathway. The antisymmetric branches, 2b, lead to equivalent antisymmetric configurations. (b) Projection of reduced gradient curve 5, notation as in part a.

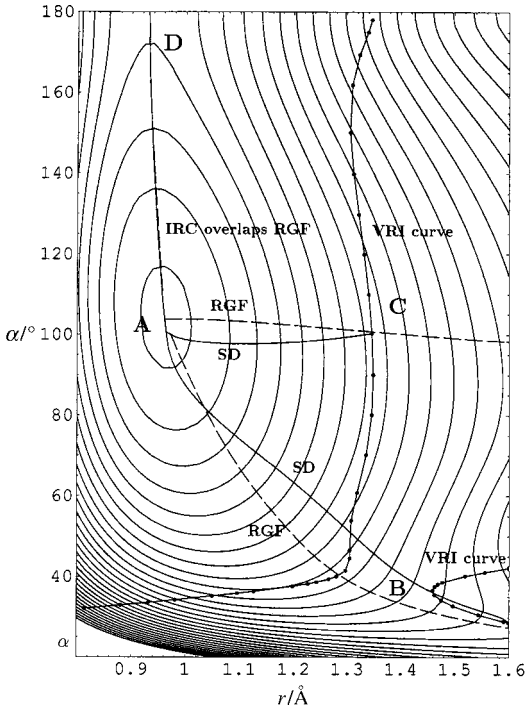

Fig. 11 Symmetric section of the PES of H_2O. RGF and steepest decent (SD) or IRC are compared.

goes up to region C along the valley of the symmetric stretch mode, see Fig. 4. The part 2a branches at the intersection with the VRI curve 1. Here, the two branches of part 2b break out of the symmetry plane. In contrast, branch 2a in Fig. 8 goes further uphill within the symmetry plane, but now along a ridge. The reduced gradient curve 3 follows the direction of the antisymmetric normal mode. One should note that in Fig. 8(a) the curves 2b and 3 do not meet. A crossing is forbidden by different gradient directions on each curve. Different curves calculated by RGF only meet where the gradient is a zero vector and this would mean at stationary points. Curve 4 starts with RGF in the bend direction and connects three parts of the PES: the SP of the linear H_2O at D, the global minimum at A, and the dissociation channel at B. There it crosses the VRI curve 1 and bifurcates into three branches which all lead to the dissociation in $O + H_2$. Curve 5 is similar to curve 4, but it fits better the symmetric reaction path of the $O + H_2$ dissociation. It is a good approximation of the MEP leading from equilibrium to the dissociation channel B. Its search direction is a combination of bending and symmetric stretch found by trial and error. "Search direction" means that at every point of the curve, which is calculated by RGF, the gradient is parallel to this direction, and *not* the tangent vector of the curve.

For a better understanding, curves 2 and 5 are depicted again in Figs. 10(a) and 10(b). The figure shows hypersurfaces of (r_1, r_2) where α is projected out of the representation. Thus, curves 2 and 5 are projected onto a plane. Curve 5 [Fig. 10(b)] follows the valley of $O + H_2$ dissociation in the direction of the bend mode, and curve 2 [Fig. 10(a)] follows the valley of the symmetric stretch to $O + H + H$. At the corresponding VRI points the ascent in the symmetric direction of both curves becomes stronger than the ascent in the direction of an antisymmetric breakout. The curves branch. Whereas parts 2a and 5a unwaveringly hold the symmetry to become a ridge, the other branches leave behind the plane of symmetry to reach the energetically favorable pathways along the valley branches. In both cases, the two directions, in which the symmetry is broken, are equivalent.

Part 2a from the minimum up to the branching point at the VRI curve may be understood as a "distinguished coordinate

path" in the direction of the symmetric stretch, representing a realistic reaction path. Beyond the branching point, the distinguished coordinate method would jump, orthogonally to the former start direction, to one of the antisymmetric branches of the curve 2b. Note that the bifurcation leads out of the symmetric plane. This holds for any symmetric curve calculated by RGF which bifurcates on the PES of H_2O. Obviously, the branching of symmetric curves on a high-dimensional PES generally takes place under loss of symmetry.

It is possible to compare RGF with steepest descent as shown in Fig. 11. One pathway of steepest descent starts at the dissociation channel in region B and runs down parallel to the reduced gradient curve 5. A second pathway of steepest descent starts at the branching point of reduced gradient curve 2 in region C. It is evident that steepest descent and RGF form close neighbouring curves in these cases. In particular, the IRC starting at the SP at D (linear structure) is near the corresponding reduced gradient curve 4. This is due to the almost linear course of the valley between minimum and SP.

5 Discussion

After finding the VRI points of a 3-dimensional test potential,[19] we used the experience for analysing the PES of a real system—the water molecule—and again we can find curves of VRI points, *i.e.* 1-dimensional manifolds. The results revise the older view of the problem,[33] which suggested that an isolated, well-defined point is obtained. The method of following a reduced gradient (RGF) as well as the alternative Branin method have succeeded in computing the VRI points. Both methods generate the same curves, although the application of both methods is different. The Branin search converges to the "next" stationary point or to a VRI point with decreasing steplength. This way allows finding these important points of the PES and a systematic search for VRI points of a given symmetry is possible. On the other hand, using the method of RGF, we are able to follow curves through large, possibly unknown parts of the configuration space with defined steplength in order to locate any stationary point or to simulate reaction path approximations.

The results reported in this paper raise the question of the meaning of high-dimensional manifolds of VRI points. Which points on the VRI manifold correspond to the chemical concept of reaction path branching? To answer this question we need a criterion that allows us to decide whether a VRI point is located on a MEP. The IRC is not defined locally and so it is unsuitable for such a task. In contrast, if a VRI point fulfills the conditions of a gradient extremal and the eigenvalues of the Hessian indicate a valley, this VRI point is located on a MEP and so this VRI point is the branching point of that reaction path. Now we will consider the reaction path which follows the symmetric $O + H_2$ dissociation of H_2O. In fact, a gradient extremal crosses the VRI curve 1 near the VRI point at (1.297 Å, 1.297 Å, 41.5°). The point is marked in Table 1. This way we can state that there is a bifurcation of the reaction path. The gradient extremal itself does not bifurcate at the crossing of the VRI line.

Finally, we will try to generalise the meaning of the curve of VRI points. A set of curves calculated by RGF referring to different search directions of the PES of H_2O is displayed in Fig. 12. Some of the curves cross the VRI manifold and branch there. The directions of their gradients can be compared with combinations of normal modes of the equilibrium structure. The curve of VRI points of the PES of H_2O may be considered as the outer limit for stable modes in the symmetric subspace, *i.e.* for H_2O the combinations of the symmetric mode and the bending. The drawback of this view is that in a real molecule a constant normal mode direction cannot be conserved, if the vibration is excited. Normal modes may change to local modes (see, *e.g.*, ref. 32).

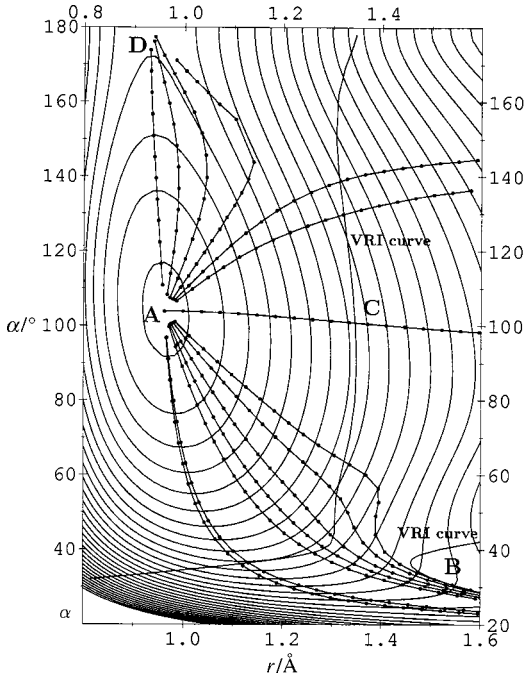

Fig. 12 Symmetric section of the PES of H_2O with reduced gradient curves to different gradient directions. Bifurcation points occur at the intersection of reduced gradient curves and VRI curves.

It has to be pointed out that the curve 1 of VRI points is sensitive to different levels of calculation. At the lower STO-3G level, this curve is not "closed" as in Figs. 8–12; however, it "opens a window" along the MEP to region B. In addition, for different polynomial fits of the PES of H_2O[34–36] there are different VRI curves.

6 The fourfold cluster problem

In the following we will compare the results of our PES analysis of H_2O with experimental results obtained from the analysis of rovibrational spectra. The discussion may be exciting for spectroscopists although it is not free of some speculation. It must be assumed that the energy ascents along vibrational motion pathways, in particular if they are accompanied by a branching, will influence the character of the spectra.

In the row of H_2X molecules (X = O, S, Se, Te, Po), so-called fourfold clusters of rotational lines are predicted;[37,38] they have already been observed for X = S and X = Se.[39] In highly excited rotational states the centrifugal forces are strong. They may cause a large distortion of the molecule away from its equilibrium configuration and then the molecule has to be treated as being nonrigid. For high values of quantum numbers J and K_a, the two highest rotational lines of the former symmetric and antisymmetric vibrational states coincide into the above-mentioned clusters, indicating the symmetry breaking of the corresponding states with lower rotational quantum number. Local mode states are the result where the rotational axis of the H_2X molecule gets closely parallel to one of the H–X bonds. In other words, the local mode vibrates along this bond axis, while the second H atom is rotating around this first H–X axis.[40] The perpendicular bond is much more affected by the centrifugal distortion. The fourfold clusters emerge for pure rotational lines of the vibrational ground state (Type I clusters)[37] as well as for the rotational lines of the ν_1/ν_3 system of stretches (Type II clusters).[41]

The fourfold Type I clusters of the vibrational ground state of water have not yet been found, see ref. 42 and references therein. Sarker *et. al.*[42] use the PES of the polynomial fit PJT_1.[34] It is less reliable in comparison with PJT_2,[35] though

Table 2 Comparison of VRI points of different molecules

Molecule	PES	$v_1 v_2 v_3$	VRI point Å	$r_{VRI} - r_e$	VRI E/cm^{-1}
$H_2{}^{16}O$	MP2[a]	—	1.346[b]	0.389	27925
$H_2{}^{16}O$	MR-CI[c]	—	1.329[b]	0.379	27600
$H_2{}^{16}O$	CCDS[d]	—	1.324	0.364	29000
$H_2{}^{16}O$	PJT_2[e]	3152/1595/3656	1.29	0.32	22950
$H_2{}^{32}S$	PJT[f]	2615/1182/2629	1.76	0.41	19750
$H_2{}^{80}Se$	KJ[g]	2344/1034/2358	1.905	0.42	17600
$H_2{}^{130}Te$	GJ[h]	2065/861/2072	2.145	0.43	16400

[a] This work. [b] A deviation of r_{VRI} of 0.01 Å causes an energy change of $\approx$500 cm^{-1}. [c] Ref. 21. [d] Ref. 36. [e] Ref. 35. [f] Ref. 47. [g] Ref. 48. [h] Ref. 49.
Note: the PESs (d) to (h) are fitted to values near the minimum; they can only be considered reliably up to about halfway to dissociation, *i.e.* the region where the VRI points are found represents a rough extrapolation of the PES.

it is also evident from Table 2 that PJT_2 is not sufficiently reliable in the region over 20000 cm^{-1}. The bond angle of the water molecule at a rotational excitation of $J = K_a = 40$, $K_c = 0$ will be reduced to about 80°.[38b,c] There, Sarker *et al.* assign an energy of 28400 cm^{-1}. This is still below the VRI point of curve 1 at 80° which is at 28630 cm^{-1}, *cf.* Table 1. We postulate that further rotational excitation could exceed the VRI line. As a consequence, the symmetric shortening should disappear and the molecule will jump into a local unsymmetrical state. Thus, the fourfold clustering should start.

The fourfold Type II clusters are experimentally observed in H_2S and H_2Se[39] where they emerge around $J = K_a = 20$ with the corresponding term values of 6618 and 5480 cm^{-1}.[43,44] The situation in H_2O, however, is not so clear or simple. The latest assignment for water shows the $J = K_a = 28$ rotational line pair of the v_1/v_3 system to be at 19552, 19514 cm^{-1} energy.[45] In H_2O, the symmetric lines cross the antisymmetric lines also at $J = K_a = 19$, but without forming fourfold Type II clusters. In Table 2 we give a comparison of H_2O, H_2S, H_2Se, and H_2Te. The VRI points used in Table 2 are found in the r_1, r_2 plane with an angle fixed at the equilibrium value of the minimum (in analogy to Fig.7). Of course, the VRI point lies on the symmetry line $r_1 = r_2$.

The PES of water is much steeper than those of the other H_2X molecules. And it shows the cirque C being a "pathway" for high-energy symmetric excitations, see Fig. 4. Keeping in mind that our *ab initio* MP2 calculation is not very reliable above half the dissociation energy (20000 cm^{-1} for water), but is much better than the surface of Table 2 (footnote *e*) (where the cirque C is missing), there still remains the fact that the VRI point for a symmetric stretch is about 10000 cm^{-1} higher in the water molecule than in the other H_2X molecules. This could explain the missing of fourfold clusters in the v_1/v_3 system of water. We postulate that the existence of the curve of VRI points is the probable reason for the instability of the symmetric modes at higher excitation, *cf.* also ref. 46. The occurrence of the fourfold clusters in the other H_2X molecules describes the pathway of redistribution of rotational states of a symmetric mode, which reach the VRI region, into a local mode valley of the PES. However, the description uses highly situated rotational states where the so-called rotational energy surface (see, for example, ref. 29) changes its shape. But the PES is the source of all molecular rigidity or even non-rigidity (as in this case). If the anharmonic structure of the PES is the reason for the change of the rotational energy surface, it is also the reason for the fourfold clusters. The water molecule should also show such features. The existence of the "closed" curve 1 (Figs. 8–12) of VRI points on the *ab initio* MP2 PES of water is a strong hint for the unavoidable loss of stability of states with $r_1 = r_2$ symmetry. The pathway of any symmetric combination mode bifurcates into two equivalent antisymmetric directions, in the corresponding α-section. Thus, any vibrational state with $r_1 = r_2$ symmetry should cease to exist if it is excited by corresponding high rotational quantum numbers: the symmetric ground state (where bending is involved at high rotational excitations), or also the stretching v_1, or its overtones, or its combination modes. In this manner, the VRI curve is the border of the accessible region of the PES for symmetric states. It is the outer edge of the funnel which collects states and directs the motions of the molecular system into the direction of a minimum energy path. Here this MEP may be the local mode direction to an unsymmetric dissociation OH + H at approximately 41000 cm^{-1}.

Acknowledgements

Our work could only have been carried out through the financial support of the Deutsche Forschungsgemeinschaft. We thank Prof. Per Jensen, Wuppertal, and Dr. Karen Keppler-Albert, Zürich, for reading the manuscript. We gratefully acknowledge the use of workstations of the Institute of Mathematics, Leipzig University.

Appendix: short description of the algorithm

We have used mass-weighted internal coordinates throughout this work. They are given by a $\boldsymbol{z}$ matrix. The corresponding $\boldsymbol{B}$ matrix has a pseudoinverse matrix $\boldsymbol{B}^+$. The contravariant metric tensor (g^{ij}) is calculated point by point taking $\boldsymbol{B}\cdot\boldsymbol{B}^+$ where the usual metric tensor (g_{ij}) forms its inverse matrix. The gradient g and the Hessian matrix $\boldsymbol{H}$ are calculated in Cartesian coordinates by the Gamess-UK package.[28] However, at any point they are transformed into their internal version by $\boldsymbol{B}^+ \cdot \boldsymbol{g}_C = \boldsymbol{g}_I$ and $\boldsymbol{B}^+ \cdot \boldsymbol{H}_C \cdot (\boldsymbol{B}^+)^T = \boldsymbol{H}_I$. Sometimes the Hessian is needed in the mixed character $(g^{ij}) \cdot \boldsymbol{H}_I$. The Hessian may be given as $[(g^{ij})^{1/2})]^T \cdot \boldsymbol{H}_I \cdot (g^{ij})^{1/2}$ for the frequency analysis, with the Cholesky decomposition[50] of (g^{ij}) into a product of an upper and a lower triangular matrix: $(g^{ij})^{1/2} \cdot [(g^{ij})^{1/2}]^T$. The eigenvalues of this Hessian matrix correspond exactly to the eigenvalues of the Cartesian Hessian $\boldsymbol{H}_C$ where, additionally, the so-called zero eigenvalues of translation and rotation emerge.

To get the system of equations for RGF, we have to define the projector $\boldsymbol{P}_r$. We calculate $(n-1)$ orthonormal direction vectors being also orthogonal to the covariant selected search direction r by using the modified Gram–Schmidt algorithm.[50] Then, the projector $\boldsymbol{P}_r$ is the matrix of these $(n-1)$ rows. Eqn. (1) for RGF becomes $\boldsymbol{P}_r \cdot \boldsymbol{H}_I \cdot \boldsymbol{t} = 0$, a linear equation for a contravariant tangent vector $\boldsymbol{t}$. It makes up the predictor step. The system is solved by QR decomposition. The reduced Hessian $\boldsymbol{P}_r \cdot \boldsymbol{H}_I$ is augmented by the covariant tangent vector to an $(n \times n)$ matrix which is the so-called $\boldsymbol{K}$ matrix.[23]

The corrector step is applied if the norm of the reduced gradient $\boldsymbol{P}_r \cdot \boldsymbol{g}_I$ is greater than a variance ϵ which is given as a parameter. The subsequent contravariant Newton–Raphson step orthogonally to the tangent is realised by solving a linear equation where the $\boldsymbol{K}$ matrix forms the left-hand side, and the right-hand side is given by the reduced gradient augmented by zero in the nth row. If the corrector steps do not converge, we

use modifications of the Newton–Raphson step; for example, the reduction of the steplength.

We may simply test the passing of a bifurcation point by comparing the tangent vector of the predictor step with the previous one. If the tangents point in opposite directions, then a bifurcation point is passed.[23] The test of a turning point is the comparison of the tangent vector of the predictor step with the direction of the first step $\boldsymbol{f}$. The comparison is realised by calculation of the inner product of these vectors with respect to the metric tensor: $t^i \cdot g_{ij} \cdot t^j_{\text{prev}}$ with respect to $t^i \cdot g_{ij} \cdot f^j$.

Either the predictor step, or the corrector step is added to the current $\boldsymbol{z}$ matrix values of the internal coordinates, and the next loop of the algorithm is begun.

References

1 K. Laidler, *Theory of Reaction Rates*, McGraw-Hill, New York, 1969.
2 H. Metiu, J. Ross, R. Silbey and T. F. George, *J. Chem. Phys.*, 1974, **61**, 3200.
3 P. Valtazanos and K. Ruedenberg, *Theor. Chim. Acta*, 1986, **69**, 281.
4 W. A. Kraus and A. E. De Pristo, *Theor. Chim. Acta*, 1986, **69**, 309.
5 P. G. Mezey, *Potential Energy Hypersurfaces*, Elsevier, Amsterdam, 1987.
6 D. Heidrich, *The Reaction Path in Chemistry: Current Approaches and Perspectives*, Kluwer, Dordrecht, 1995.
7 D. Heidrich, W. Kliesch and W. Quapp, *Properties of Chemically Interesting Potential Energy Surfaces*, Springer, Berlin, 1991.
8 J. Baker and P. M. W. Gill, *J. Comput. Chem.*, 1988, **9**, 465.
9 K. Fukui, *J. Phys. Chem.*, 1970, **74**, 4161.
10 A. Tachibana and K. Fukui, *Theor. Chim. Acta*, 1978, **49**, 321.
11 W. Quapp, *J. Chem. Soc., Faraday Trans.*, 1994, **90**, 1607.
12 M. V. Basilevsky and A. G. Shamov, *Chem. Phys.*, 1981, **60**, 337, 347.
13 D. J. Rowe and A. Ryman, *J. Math. Phys.*, 1982, **23**, 732.
14 D. K. Hoffman, R. S. Nord and K. Ruedenberg, *Theor. Chim. Acta*, 1986, **69**, 265.
15 M. V. Basilevsky, *Chem. Phys.*, 1982, **67**, 337.
16 W. Quapp, *Theor. Chim. Acta*, 1989, **75**, 447.
17 W. Quapp, M. Hirsch, O. Imig and D. Heidrich, *J. Comput. Chem.*, 1998, **19**, 1087.
18 I. H. Williams and G. M. Maggiora, *J. Mol. Struct.* (*Theochem*), 1982, **89**, 365.
19 W. Quapp, M. Hirsch and D. Heidrich, *Theor. Chem. Acc.*, 1998, **100**, 285.
20 H. T. Jongen, P. Jonker and F. Twit, in *Parametric Optimization and Related Topics*, ed. J. Guddat, H. T. Jongen, B. Kummer and F. Nozicka, Akademie-Verl., Berlin, 1987, p. 209.
21 T. S. Ho, T. Hollebeek, H. Rabitz, L. B. Harding and G. C. Schatz, *J. Chem. Phys.*, 1996, **105**, 10472.
22 I. Diener, *Globale Aspekte des kontinuierlichen Newton-Verfahrens*, Habilitation, Göttingen, 1991.
23 E. L. Allgower and K. Georg, *Numerical Continuation Methods—An Introduction*, Springer, Berlin, 1990.
24 K. Müller and L. D. Brown, *Theor. Chim. Acta*, 1979, **53**, 75.
25 S. Wolfram, *MATHEMATICA*, *Ver. 2.2*, Wolfram Research, Champain, IL, 1993.
26 F. H. Branin, *IBM J. Res. Develop.*, 1972, **16**, 504.
27 S. Ackermann and W. Kliesch, *Theor. Chem. Acc.*, 1998, **99**, 255.
28 M. F. Guest, P. Fantucci, R. J. Harrison, J. Kendrick, J. H. van Lenthe, K. Schoeffel and P. Sherwood, *GAMESS-UK Program*, Revision C.0, CFS Ltd., Daresbury Laboratory, 1993.
29 W. G. Harter, *Principles of Symmetry, Dynamics and Spectoscopy*. John Wiley & Sons, New York, 1993.
30 K. Ruedenberg and J.-Q. Sun, *J. Chem. Phys.*, 1994, **100**, 5836.
31 W. Quapp, O. Imig and D. Heidrich, in *The Reaction Path in Chemistry: Current Approaches and Perspectives*, ed. D. Heidrich, Kluwer, Dordrecht, 1995, p. 137.
32 (*a*) M. S. Child and R. T. Lawton, *Mol. Phys.*, 1981, **44**, 709; (*b*) B. R. Henry, *Acc. Chem. Res.*, 1977, **10**, 207; (*c*) L. Halonen, *J. Chem. Phys.*, 1987, **88**, 4171; (*d*) I. M. Mills and A. G. Robiette, *Mol. Phys.*, 1985, **56**, 743; (*e*) J. B. Rose and M. E. Kellman, *J. Chem. Phys.*, 1996, **105**, 7348.
33 (*a*) A. Tachibana, I. Okazaki, M. Koizumi, K. Hore and T. Yamabe, *J. Am. Chem. Soc.*, 1985, **107**, 1190; (*b*) B. J. Smith, D. J. Swanton, J. A. Pople, H. F. Schaefer and L. Radom, *J. Chem. Phys.*, 1990, **92**, 1240; (*c*) R. G. A. Bone, T. W. Rowlands, N. C. Handy and A. J. Stone, *Mol. Phys.*, 1991, **72**, 33; (*d*) R. G. A. Bone, *Chem. Phys. Lett.*, 1992, **193**, 557; (*e*) T. Taketsugu and T. Hirano, *J. Chem. Phys.*, 1993, **99**, 9806; (*f*) R. G. A. Bone, *Chem. Phys.*, 1993, **178**, 255; (*g*) T. Taketsugu and T. Hirano, *J. Mol. Struct.* (*Theochem*), 1994, **130**, 169; (*h*) J. L. Liao, H. L. Wang and H. W. Xin, *Chin. Sci. Bull.*, 1995, **40**, 566; (*i*) T. Taketsugu and M. S. Gordon, *J. Chem. Phys.*, 1995, **103**, 10042; (*k*) Y. Yanai, T. Taketsugu and T. Hirano, *J. Chem. Phys.*, 1997, **107**, 1137; (*l*) G. V. Shustov and A. Rauk, *J. Org. Chem.*, 1998, **63**, 5413.
34 O. L. Polyansky, P. Jensen and J. Tennyson, *J. Chem. Phys.*, 1994, **101**, 7651.
35 O. L. Polyansky, P. Jensen and J. Tennyson, *J. Chem. Phys.*, 1996, **105**, 6490.
36 G. de Olivera and C. E. Dykstra, *Theor. Chem. Acc.*, 1999, **101**, 435.
37 I. N. Kozin, S. Klee, P. Jensen, O. L. Polyansky and I. M. Pavlichenko, *J. Mol. Spectrosc.*, 1993, **158**, 409.
38 (*a*) B. I. Zhilinskii and I. M. Pavlichenko, *Opt. Spektrosc.*, 1988, **64**, 413; (*b*) I. N. Kozin and I. M. Pavlichenko, *J. Chem. Phys.*, 1996, **104**, 4105; (*c*) J. Makarewicz, *J. Chem. Phys.*, 1997, **108**, 469; (*d*) P. R. Bunker and P. Jensen, *Molecular Symmetry and Spectroscopy*, NRC Research Press, Ottawa, 1998.
39 J. M. Flaud, C. Camy-Peyret, H. Bürger, P. Jensen and I. N. Kozin, *J. Mol. Spectrosc.*, 1995, **172**, 126.
40 M. S. Child, O. V. Naumenko, M. A. Smirnov and L. R. Brown, *Mol. Phys.*, 1997, **92**, 885.
41 I. N. Kozin and P. Jensen, *J. Mol. Spectrosc.*, 1993, **161**, 186.
42 P. Sarker, N. Poulin and T. Carrington Jr., *J. Chem. Phys.*, 1999, **110**, 10269.
43 I. N. Kozin and P. Jensen, *J. Mol. Spectrosc.*, 1994, **163**, 483.
44 I. N. Kozin and P. Jensen, *J. Mol. Spectrosc.*, 1993, **160**, 39.
45 O. L. Polyansky, J. Tennyson and N. F. Zobov, *Spectrochim. Acta A*, 1999, **55**, 659.
46 (*a*) W. L. Hase, *J. Phys. Chem.*, 1986, **90**, 365; (*b*) K. Stefanski and E. Pollak, *J. Chem. Phys.*, 1997, **87**, 1079; (*c*) G. M. Schmid, S. L. Coy, R. W. Field and R. J. Silbey, *J. Chem. Phys.*, 1994, **101**, 869.
47 O. L. Polyansky, P. Jensen and J. Tennyson, *J. Mol. Spectrosc.*, 1996, **178**, 184.
48 I. N. Kozin and P. Jensen, *J. Mol. Spectrosc.*, 1993, **160**, 46.
49 P. C. Gómez and P. Jensen, *J. Mol. Spectrosc.*, 1997, **185**, 282.
50 A. Kiełbasiński and H. Schwetlick, *Numerische Lineare Algebra*, VEB Deutscher Verlag der Wissenschaften, Berlin, 1988.

Paper 9/05926A